

See discussions, stats, and author profiles for this publication at: <https://www.researchgate.net/publication/261740817>

Charged Polymer Brushes-Grafted Hollow Silica Nanoparticles as a Novel Promising Material for Simultaneous Joint Lubrication and Treatment

ARTICLE in THE JOURNAL OF PHYSICAL CHEMISTRY B · APRIL 2014

Impact Factor: 3.3 · DOI: 10.1021/jp500074g · Source: PubMed

CITATIONS

7

READS

43

4 AUTHORS, INCLUDING:



Guoqiang Liu

Chinese Academy of Sciences

14 PUBLICATIONS 127 CITATIONS

[SEE PROFILE](#)



Meirong Cai

Chinese Academy of Sciences

26 PUBLICATIONS 274 CITATIONS

[SEE PROFILE](#)



Feng Zhou

Chinese Academy of Sciences

257 PUBLICATIONS 6,295 CITATIONS

[SEE PROFILE](#)

Charged Polymer Brushes-Grafted Hollow Silica Nanoparticles as a Novel Promising Material for Simultaneous Joint Lubrication and Treatment

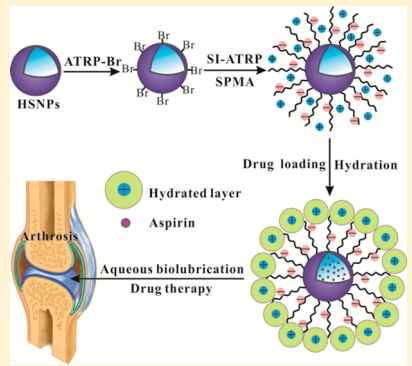
Guoqiang Liu,^{†,‡} Meirong Cai,^{*,†} Feng Zhou,^{*,†} and Weimin Liu[†]

[†]State Key Laboratory of Solid Lubrication, Lanzhou Institute of Chemical Physics, Chinese Academy of Sciences, Lanzhou 730000, Gansu, China

[‡]Graduate School of Chinese Academy of Sciences, Beijing 100039, China

S Supporting Information

ABSTRACT: The fabrication of core/shell charged polymer brushes-grafted hollow silica nanoparticles (PSPMA-g-HSNPs) is reported. Because of the excellent hydration capability of the shells consisting of charged polymer brushes, the functional nanoparticles can achieve a good lubricating effect in aqueous media via hydration lubrication mechanism. The mesoporous hollow silica cores endow the nanoparticles with drug loading–release capability. Aspirin, as a useful drug for treating arthritis, was employed to carry out *in vitro* drug loading and release studies. It is clear that brushes-modified hollow silica exhibited long-term drug release performance. The combination of lubrication and drug loading capabilities results in the great clinical potential of new multifunctional nanoparticles as injectable joint lubricant fluid in arthritis treatment.



1. INTRODUCTION

Excellent lubrication between the articular cartilage surfaces is responsible for the proper motion of human hips or knees, and the failure of the lubrication will cause osteoarthritis.^{1,2} More than 50% of the population ultimately suffers the pains of osteoarthritis because damaged or worn articular cartilage has limited capability of self-healing because of the low chondrocytes density.³ In this case, both sufficient lubrication and proper treatment are important for prevention and amelioration of degradative performance of human joints. To achieve this goal, therapy treatment by injectable joint lubricant fluid together with medicine may be an effective approach.^{4,5} Multifunctional nanospheres have been widely studied in various fields, including bioseparation, energy storage, smart sensors, and bioimaging,^{6–11} and may be a promising candidate for both joint lubrication and drug treatment.

Development of artificial biolubrication fluid was inspired by nature.^{12,13} The main ingredients of human synovial fluid, including hyaluronan, aggrecan, and glycoproteins lubricin, are all brush-like polyelectrolyte biomacromolecules.^{14,15} Water is the natural media of living systems, so biological lubrication is achieved by hydration lubrication,¹⁶ which is provided by the hydration layers surrounding charges.^{17,18} Inspired by this concept, charged polymer brushes are clearly appropriate model materials for biological lubrication,^{12,19–21} and the hydrated layer was formed surrounding the ions in aqueous media.^{22,23} Aqueous biolubrication by polymer brushes chemically grafted on planar substrates as an artificial biomimicking system has been widely studied, and superlow friction

coefficients have been achieved thereon.^{24–27} However, the translation of charged polymer brushes to its application of brush-like additive in joint lubricating fluid is very rare.

To this end, we aim to explore the application of spherical charged polymer brushes-grafted nanoparticles in aqueous biolubrication. Compared with conventional lubricant additives, micro- and nanometer-sized spherical particles with small size effect and special physicochemical properties have unique advantages in the field of aqueous lubrication.^{28–31} In addition, nanospheres may employ a “rolling” mechanism to reduce friction between sliding surfaces.³² Over the years, spherical polymer brushes have been investigated for various applications, including chromatography,³³ enrichment of phosphopeptides,³⁴ protein resistant materials,³⁵ self-healing coatings,³⁶ and water remediation.³⁷ However, spherical charged polymer brushes-grafted nanoparticles as a biomimetic lubricant have never been reported, which is of special interest in tribology. In our work, negatively charged poly(3-sulfopropyl methacrylate potassium salt) (PSPMA) brushes were employed as the outer layer of designed composite nanoparticles to provide hydration lubrication. The PSPMA brushes surrounding the nanospheres have strong hydration capability, can be fully extended in aqueous media,^{38,39} and meanwhile play a central role in colloid stabilization because of electrostatic and steric interactions.

Received: January 3, 2014

Revised: April 4, 2014

Published: April 15, 2014



Concurrent with good lubrication, there is also strong demand for achieving medical treatment using lubricating materials that are able to deliver medicine in a controlled release manner. Hollow spherical silica nanoparticles (HSNPs) can be a candidate as the cores of designed composite nanoparticles to achieve controlled drug release.^{40,41} Because of good biocompatibility, unique chemical properties, and convenient surface modification, HSNPs have been used in various biomedical fields including protection for proteins, drug delivery, artificial cells, and large biomolecular release systems.^{42–44}

In our work, negatively charged PSPMA brushes-grafted hollow silica nanoparticles (PSPMA-g-HSNPs) with dual functions of hydration lubrication and drug delivery were introduced. HSNPs were employed as the cores of the designed composite nanoparticles to load and release drugs. On the outer layer of HSNPs, an anionic PSPMA polymer brush was grafted to provide hydration lubrication. Friction and wear tests show that the composite nanoparticles possess a good lubricating effect in aqueous media via a hydration lubrication mechanism. *In vitro* cytotoxicity demonstrated that the PSPMA-g-HSNPs were biocompatible, making them suitable for biomedical applications. *In vitro* drug loading and release were conducted using aspirin as a model drug in the human physiological environment, indicating the suitability as the drug loading and sustained-release carrier. Our study may be a novel approach for designing injectable joint lubricant fluid for simultaneous joint lubrication and treatment.

2. EXPERIMENTAL SECTION

2.1. Materials. Styrene (St, AR grade), toluene, and ammonium hydroxide (28–30 wt %) were purchased from Shanghai Chemical Reagent Co. Tetraethyl orthosilicate (TEOS, reagent grade, 98%) and polyvinylpyrrolidone (PVP40; average MW, 40 000) were purchased from Sigma-Aldrich. 3-Sulfopropyl methacrylate potassium salt (SPMA, 98%), 2,2'-bipyridine (Bpy, 99%), and copper(I) bromide (CuBr) were purchased from TCI Co., Ltd. Rhodamine B (RHB, 96%) and aspirin (98%) were purchased from J&K. Prior to use, St was washed with NaOH aqueous solution (5 wt %) and deionized water several times to remove the inhibitor, and CuBr was refluxed overnight in acetic acid. Toluene was dried by distillation over CaH₂. Other chemicals were used with no treatment. Initiator 3-(trichlorosilyl)propyl-2-bromo-2-methylpropanoate was synthesized in the group.

2.2. Preparation of Hollow Silica Particles. The typical preparation process of HSNPs was as follows. The template of polystyrene (PS) particles was first fabricated via emulsifier-free emulsion polymerization, where St (10.0 g), PVP (1.5 g), AIBA (0.26 g), and H₂O (100.0 g) were added into a four-neck round-bottom flask (250 mL), deoxygenated for 60 min, and heated at 70 °C for 24 h with stirring at 300 rpm. The resultant PS dispersion was purified by dialysis and then used as templates to prepare the HSNPs. TEOS (1.0 g) and ammonium hydroxide (5.0 mL) were dissolved in 40 mL of anhydrous ethanol in a round-bottom flask (100 mL). Then, PS dispersion (3.5 g) was added into the solution. The HSNPs were formed by the sol–gel reaction at 50 °C for 1.5 h. Interestingly, when silica shells formed around the PS cores, the PS cores were dissolved by ammonia. Thus, the hollow structure formed without additional dissolution or calcination.^{45,46} The HSNPs was collected by centrifugation and

washed with water and ethanol. Finally, the sample was dried under vacuum overnight.

2.3. Immobilization of ATRP Initiator. The atom transfer radical polymerization (ATRP) initiator was immobilized onto the surface of silica particles via a hydrolysis–condensation process. HSNPs (20 mg), anhydrous toluene (20 mL), and ATRP initiator (5 μL) were put into a round-bottom flask (50 mL) and magnetically stirred at room temperature overnight. Then the initiator-immobilized hollow silica particles were collected by centrifugation and washed with fresh anhydrous toluene and dichloromethane several times. Finally, the obtained nanoparticles were dried under vacuum at room temperature overnight.

2.4. Synthesis of PSPMA Brushes-Grafted HSNPs by Surface-Initiated ATRP. The PSPMA-g-HSNPs were prepared via surface-initiated ATRP. Typically, the initiator-immobilized HSNPs (20 mg) and SPMA (1.5 g) were dispersed in 8 mL of 1:1 (v:v) MeOH/H₂O by 5 min of ultrasonication in a glass tube. The dispersion was deoxygenated for 30 min before the 2,2'-bipyridyl (0.0625 g, 0.4 mmol) and CuBr (0.0287 g, 0.2 mmol) were added to initiate the ATRP. Then, the polymerization was conducted at room temperature under N₂ protection for 2 h. Finally, the PSPMA-g-HSNPs were collected by centrifugation and purified with deionized water and ethanol several times. Finally, the resultant composites were dried under vacuum overnight. To remove the copper catalyst, the sample was purified in a dialysis tube (molecular weight cutoff at 12 kDa, Sigma-Aldrich) with 1000 mL of deionized water for 72 h, and the water was exchanged at intervals of 12 h.

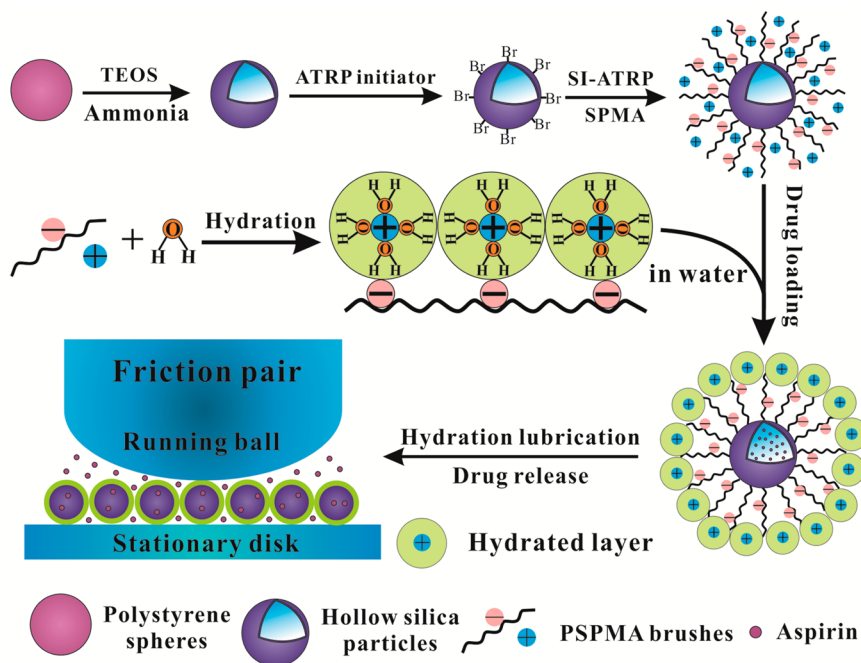
2.5. Chemical Structure Analysis. Fourier transform infrared (FTIR) spectra were recorded on the Perkin-Elmer Spectrum one Transform Infrared Spectrometer (PerkinElmer, U.S.). The thermal properties were studied on an STA 449 C Jupiter simultaneous TG-DSC instrument. X-ray photoelectron spectra (XPS) were recorded by a XPS/AES system (Model PHI-5072, Physical Electronics, Inc., Eden Prairie, MN).

2.6. Morphology, Particle Size, and Specific Surface Area Characterization. Field emission transmission electron microscopy (TEM, FEI, Tecnai, G2 TF20) and field emission scanning electron microscopy (SEM, JSM-6701F, JEOL, Japan) were employed to observe the morphology and size of PS, HSNPs, and PSPMA-g-HSNPs. The surface compositions of HSNPs and PSPMA-g-HSNPs were analyzed using energy-dispersive X-ray spectroscopy (EDXS). The Brunauer–Emmett–Teller (BET) measurement was performed on an ASAP 2020 (Micromeritics Instruments, U.S.) nitrogen adsorption instrument. Prior to the measurement, the HSNPs and PSPMA-g-HSNPs were both degassed at 150 °C for several hours.

The dynamic light scattering technique (DLS) was employed to measure hydrodynamic diameters and ζ -potential of PSPMA-g-HSNPs on a particle size analyzer (Zetasizer Nano ZS, Malvern Instruments, U.K.) equipped with a 633 nm He–Ne laser. The swelling ratio (SR) was calculated by the following equation: SR = $V_{\text{aqueous}}/V_{\text{dry}} = (D_{\text{aqueous}}/D_{\text{dry}})^3$, where V_{aqueous} and V_{dry} are the volumes of swollen PSPMA-g-HSNPs in aqueous media and shrunken PSPMA-g-HSNPs in the dry state, respectively. D_{aqueous} and D_{dry} are the mean diameters of PSPMA-g-HSNPs from DLS and TEM, respectively.

2.7. In Vitro Cytotoxicity Test. Cell cytotoxicity studies were determined at different concentrations by standard MTT assays, and HeLa cells were used. The cells were first placed in

Scheme 1. Fabrication of PSPMA-g-HSNPs, Hydration Mechanism of Negatively Charged Polymer Brushes, Drug Loading and Release, and Hydration Lubrication between Steel and Steel Contacts



96-well plates at a density of 2.5×10^4 cells/well and then incubated in a standard culture for 24 h. Afterward, the cells were exposed to PSPMA-g-HSNPs with different concentrations and incubated for 48 h. MTT (5 mg/mL, 20 mL/well) was then added to the growth medium, and the cells were incubated for another 4 h at 37 °C. After the removal of the supernatant, dimethyl sulfoxide (DMSO, 150 mL/well) was added and the plates were agitated to completely dissolve the crystals. The absorbance was recorded using a microplate reader at 570 nm. The results were obtained from the mean values of three parallel measurements, and the cell viability was evaluated by the following formula: Cell viability (%) = $OD_{570(\text{sample})}/OD_{570(\text{control})} \times 100$, where $OD_{570(\text{sample})}$ represents the optical density (OD) of treated cells and $OD_{570(\text{control})}$ represents that of untreated control cells.

2.8. Rheological Characterization. The rheological behavior of PSPMA-g-HSNP aqueous suspension was investigated by an RS6000 Rheometer (Germany) using a parallel-plate geometry (diameter, 35 mm; gap, 1 mm) at 25 °C. The concentration of PSPMA-g-HSNP suspension was 0.3 wt %, and the amount of the suspension dropped on the plate was 1.0 mL. The viscosity versus shear rate curve and the shear stress versus shear rate curve were obtained using a shearing mode. An oscillatory stress sweep with a controlled frequency (1 Hz) was used for measuring G' and G'' .

2.9. Friction and Wear Tests. The tribological properties tests were performed on an Optimol SRV-IV oscillating reciprocating friction and wear tester. The ball-on-block configuration was adopted in the tests. The diameters of the upper running ball and the lower stationary disk are 10 mm and 24 mm, respectively. The measurement was performed at amplitude of 1 mm and frequency of 25 Hz. The relative humidity was 20–35%. The elastic modulus of steel used in the friction test was 190–210 GPa, and the Hertzian maximum contact pressure was 1.66 GPa (50 N), 2.10 GPa (100 N), 2.40 GPa (150 N), and 2.64 GPa (200 N). The wear volume on the

lower disk was measured by a MicroXAM 3D noncontact surface mapping profiler.

2.10. Absorption Studies by Fluorescence Microscopy. To study the absorption of PSPMA-g-HSNPs on the steel–steel contacts, PSPMA-g-HSNPs were labeled with Rhodamine B (RHB). The dyeing process was as follows. PSPMA-g-HSNPs (10 mg) was dispersed ultrasonically in 10 mL of RHB aqueous solution (1.0 mg/mL), and the mixture was stirred in a flask for 24 h. Then, the RHB-labeled PSPMA-g-HSNPs were collected by centrifugation, washed with ultrapure water several times, and dried under vacuum at room temperature for 24 h. The dry labeled PSPMA-g-HSNPs were redispersed in a certain amount of water. Some steel blocks were freshly polished for further use. A drop of labeled PSPMA-g-HSNP suspension (0.3 wt %) was dropped on the steel block. The steel blocks were incubated for 1.0 h in order to carry out an absorption process. After incubation, the steel blocks were washed using ultrapure water and dried by nitrogen flow. Finally, the absorption of labeled PSPMA-g-HSNPs on the steel block was observed by fluorescence microscopy. The absorption of labeled PSPMA-g-HSNP suspension with different concentrations (0.1, 0.3, and 0.5 wt %) within 1.0 h was studied using the same method.

2.11. Preparation of Calibration Curves. Aspirin was dissolved in PBS buffer solution (pH 7.4) and diluted to different concentrations. The UV absorbance of aspirin solutions was recorded on a UV-vis spectrophotometer (Cary 60 UV-Vis, Agilent Technologies) at 297 nm, and then the calibration curve was drawn based on the UV absorption.

2.12. Fabrication of Drug-Loaded PSPMA-g-HSNPs. The drug loading and in vitro release profiles were obtained by the reported methods.^{47,48} Aspirin was employed as a drug model. To load aspirin into the PSPMA-g-HSNPs, aspirin (20 mg) and PSPMA-g-HSNPs (20 mg) were added to 20 mL of ethanol/water ($v:v = 1:1$) solution in a flask at room

temperature. The PSPMA-g-HSNPs were dispersed uniformly by ultrasound, and then the mixture was stirred at 25 °C for 48 h. The aspirin-loaded PSPMA-g-HSNPs were separated by centrifugation, purified with ethanol/water several times, and dried under vacuum at 60 °C. Meanwhile, the aspirin-loaded HSNPs were also prepared using the same method as that of the reference. The amount of aspirin was analyzed using UV-vis spectrophotometer at a wavelength of 297 nm. The measurement was performed in triplicate for each sample to ensure the accuracy. The drug loading capacity (LC) and encapsulation efficiency (EE) were evaluated by the following formulas, respectively.

$$\text{LC}(\%) = \frac{\text{amount of loaded aspirin}}{\text{amount of aspirin} - \text{loaded PSPMA-g-HSNPs}} \times 100\%$$

$$\text{EE}(\%) = \frac{\text{amount of loaded aspirin}}{\text{total amount of added aspirin}} \times 100\%$$

2.13. In Vitro Drug Release. The in vitro release behavior of aspirin from PSPMA-g-HSNPs at room temperature was conducted by the dialysis tube diffusion technique, and free aspirin and aspirin-loaded HSNPs were used as the references. The drug-loaded nanoparticles were put into a dialysis tube (molecular weight cutoff, 8 000–10 000). Then the tube was dialyzed against the 250 mL of phosphate buffer solution (pH 7.4) at 37 °C. After a fixed time, 3 mL of the medium was taken out and replaced by 3 mL of fresh PBS solution. The amount of released aspirin was evaluated by UV absorption. The release percent of aspirin was calculated using the following equation:

$$\text{drug release (\%)} = \frac{M_t}{M_\infty} \times 100\%$$

Where M_t is the amount of aspirin released from the as-prepared nanoparticles at time t and M_∞ is the complete amount of aspirin released, respectively.

3. RESULTS AND DISCUSSION

The experimental design is illustrated in Scheme 1. The synthesis of PSPMA-g-HSNPs consists of three steps. First, HSNPs were prepared according to the literature with little modification.⁴¹ Second, the ATRP initiator was immobilized onto the surface of silica particles via a hydrolysis–condensation process. Third, the PSPMA-g-HSNPs were synthesized by surface-initiated ATRP. The chemical composition and morphology of the composite nanoparticles were well-defined by FTIR, XPS, and thermogravimetric analysis (TGA). The successful grafting of PSPMA brushes on HSNPs and the excellent swelling capacity were confirmed by TEM and DLS, respectively. Rheological characterization, friction and wear test, and surface absorption analysis were employed to investigate the hydration lubrication of the composite nanoparticles. In vitro cytotoxicity was investigated by an MTT assay using HeLa cell lines. In vitro drug loading and release were conducted using aspirin as a model drug in the human physiological environment.

3.1. FTIR and XPS Characterization. Figure 1 depicts the FTIR spectra of HSNPs, HSNPs-Br and PSPMA-g-HSNPs. For HSNPs, the characteristic absorption peak of Si–O–Si appears at 1093 cm⁻¹. The peak at 3425 cm⁻¹ is assigned to the stretching absorption vibration of Si–OH, indicating that the as-prepared HSNPs are rich in hydroxyl groups. Compared

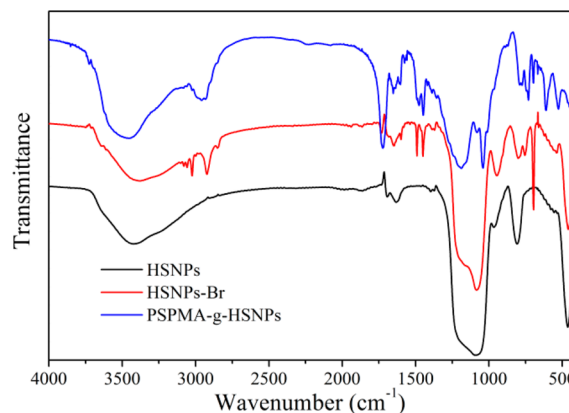


Figure 1. FTIR spectra of HSNPs, HSNPs-Br, and PSPMA-g-HSNPs.

with the FTIR spectrum of HSNPs, some new peaks of HSNPs-Br are observed. The absorption band at 3026–2840 cm⁻¹ is assigned to the stretching vibration of C–H in –CH₃ and –CH₂–, whereas the peaks at 1493 and 1453 cm⁻¹ are attributed to the bending vibration of C–H in –CH₃ and –CH₂–. It is important that the characteristic absorption peaks of C=O and C–Br in acyl bromide groups appear at 1648 and 698 cm⁻¹, suggesting the siloxane initiator was successfully attached to HSNPs. Then the PSPMA brushes were grafted from the surface of HSNPs via SI-ATRP. The characteristic absorption peaks of S=O in SO₃⁻ groups appear at 1190 and 1042 cm⁻¹, whereas the strong absorption peak at 1725 cm⁻¹ arises from C=O in ester groups. The appearance of these absorption peaks confirms that polymer brushes have been grafted onto HSNPs.

The surface chemical nature of HSNPs, HSNPs-Br, and PSPMA-g-HSNPs was further established by XPS analysis in Figure 2. In Figure 2a, the binding energies of Si 2p and Si 2s at 104 and 155 eV were assigned to the silica shells of HSNPs. In Figure 2b, the appearance of a signal for Br 3d and Br 4s at 71 and 26 eV indicated that the successful immobilization of the ATRP initiator onto the surface of HSNPs. In Figure 2c, the successful grafting of PSPMA brushes onto the HSNPs was verified by the presence of signals for K 2s (377 eV), K 2p (293 eV), S 2s (232 eV), and S 2p (168 eV).

3.2. Thermogravimetric Analysis. Figure 3 shows the TGA thermograms obtained from HSNPs, HSNPs-Br, and PSPMA-g-HSNPs. Because of hydroxyls on the surface of HSNPs, pure HSNPs contain a certain amount of bound water, which will be lost during the heating process. A weight loss of 8.5% can be observed from the curve of HSNPs. After the immobilization of the initiator, the weight loss of HSNPs-Br is ca. 12.1% and the content of the initiator is calculated to be 3.6%. Moreover, after PSPMA is grafted by ST-ATRP, the weight loss of PSPMA-g-HSNPs was increased to 67.5% and the content of PSPMA brushes is calculated to ca. 55.4%. TGA thermograms provide a quantitative analysis for each component of PSPMA-g-HSNPs.

3.3. Morphology Characterization. The morphology of PS, HSNPs, and PSPMA-g-HSNPs was observed via TEM and SEM. As shown in Figure 4a,b, PS templates are uniform in size with the diameter of ca. 286 nm. After the sol–gel reaction and the removal of PS templates, the hollow silica particles (Figure 4c) were formed with the average diameter of ca. 342 nm. The high contrast between the dark shells and light cavities indicates that PS templates were completely removed in the HSNPs. The

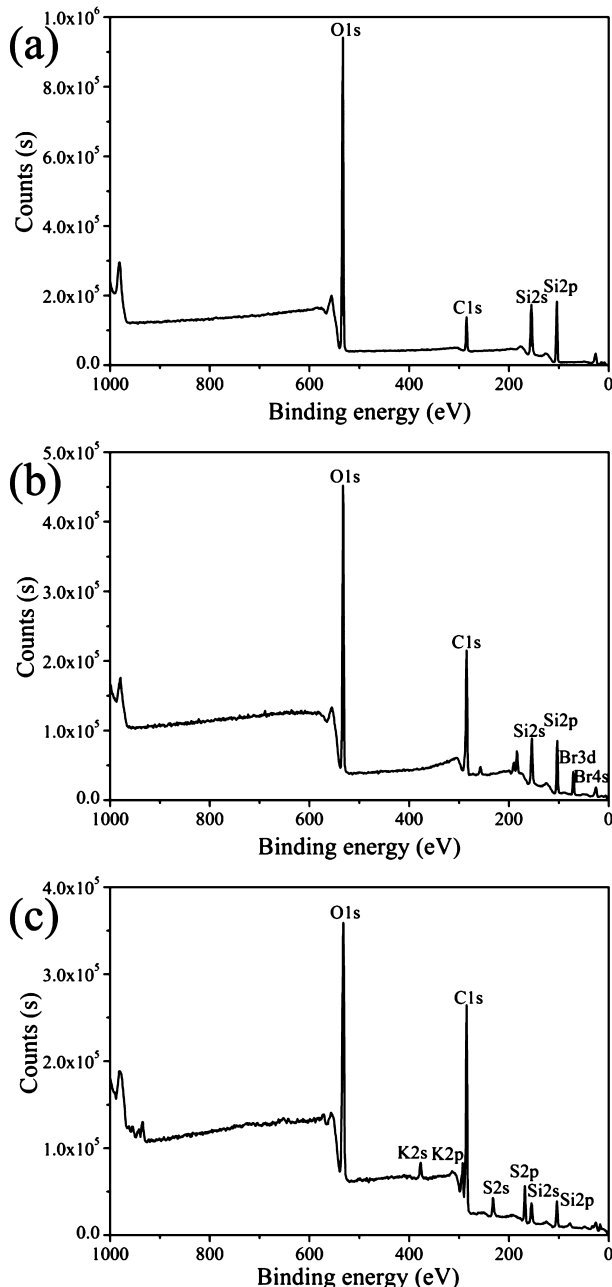


Figure 2. XPS survey spectra of HSNPs (a), HSNPs-Br (b), and PSPMA-g-HSNPs (c).

thickness of the silica shell was ca. 28 nm. Afterward, the PSPMA-g-HSNPs were prepared through immobilization of initiator and surface-initiated ATRP. As shown in Figure 4d, it is quite evident that the HSNPs were surrounded by a shaded polymer layer with a thickness of ca. 40 nm. The diameter of the composite particles was increased to ca. 422 nm. TEM results indicate the HSNPs were successfully coated by PSPMA brushes.

To confirm the elemental composition of the obtained nanoparticles, EDXS analysis was conducted on a FEI TF20 TEM instrument. As shown in Figure 4e, the EDXS spectra of HSNPs display the appearance of only Si and O signals, suggesting the complete removal of PS templates. Compared with that of HSNPs, EDXS analysis of PSPMA-g-HSNPs in Figure 4f showed the presence of S and K signals, which

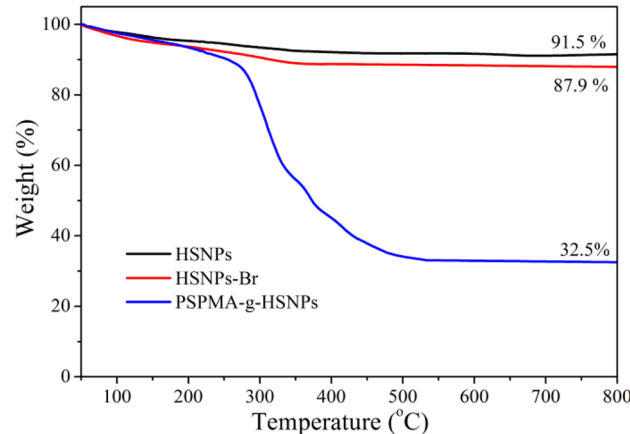


Figure 3. TGA curves of HSNPs, HSNPs-Br, and PSPMA-g-HSNPs.

indicates the successful grafting of PSPMA brushes onto the surface of HSNPs.

3.4. BET Measurement. To further investigate the porosity of HSNPs and PSPMA-g-HSNPs, the N_2 adsorption–desorption isotherms of HSNPs and PSPMA-g-HSNPs and the corresponding pore size distribution curves were measured by the BET method (Figure 5). The specific surface area of pure HSNPs can reach $192.5\text{ m}^2/\text{g}$, and the pore size distribution is relatively narrow with a peak at 3.5 nm. The isotherms in the range of $0.5\text{--}1.0\text{ P/P}_0$ show an obvious hysteresis loop and can be assigned to type IV, indicating the existence of mesoporous structures in the HSNPs. Because of the hollow cavity, the HSNPs can load a large amount of substance. Importantly, the nanopores in the shells provide channels for drug molecules to penetrate into the interior cavity, and subsequently the drug can release outside the HSNPs.

From the pore size distribution curves, the pore volume of PSPMA-g-HSNPs is much smaller than that of HSNPs in the range of 0–100 nm. The BET surface area of PSPMA-g-HSNPs was calculated to be $8\text{ m}^2/\text{g}$, indicating that the channels of the silica shell were almost completely blocked by PSPMA brushes in dry conditions. However, PSPMA brushes cannot prevent outer molecules from loading into the interior cavity of HSNPs in an aqueous environment. The stretch of PSPMA brushes in water can open the pores of HSNPs, which is investigated by the subsequent DLS measurement.

3.5. Dynamic Light Scattering. The hydrodynamic diameter and ζ -potential of PSPMA-g-HSNPs were measured by DLS. Figure 6 shows the hydrodynamic diameter distribution by intensity (Figure 6a) and the ζ -potential distribution (Figure 6b) of PSPMA-g-HSNPs in aqueous media at 25 °C.

The hydrodynamic diameter of PSPMA-g-HSNPs is ca. 739.2 nm (Figure 6), which is much larger than that in the dry condition (ca. 420 nm, via TEM). Because of the hydration of PSPMA brushes, the polymer chains can be fully extended in aqueous media, resulting in a good swelling capability of PSPMA-g-HSNPs. The swelling ratio ($V_{\text{aqueous}}/V_{\text{dry}}$) is calculated to be 5.45. The ζ -potential of PSPMA-g-HSNPs is -57.6 mV after the coverage of charged PSPMA brushes, suggesting good dispersibility ($\text{PDI} = 0.296$) and stability because of electrical interaction. DLS results suggest a strong hydrated capability and a good swelling performance of PSPMA-g-HSNPs.

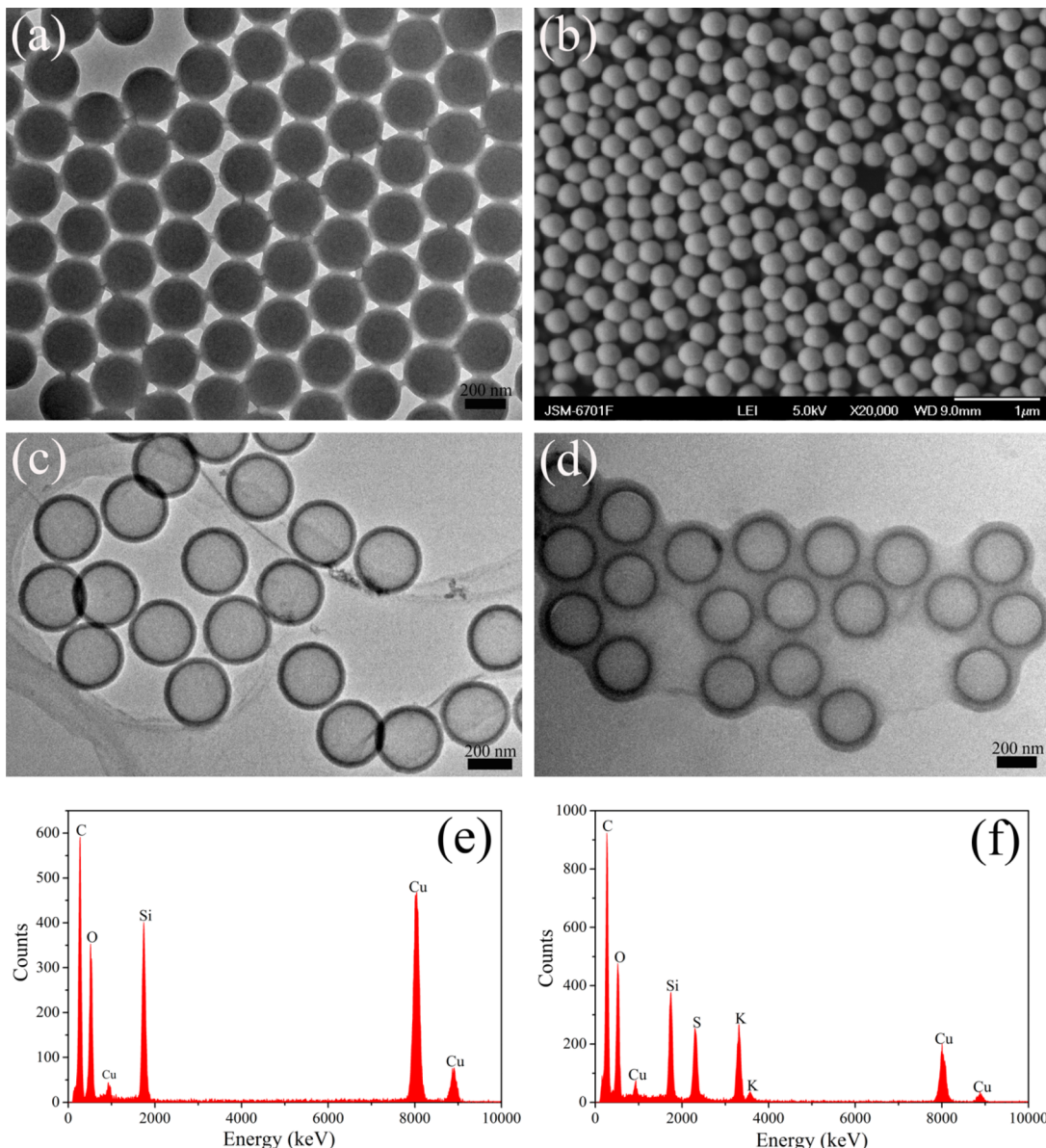


Figure 4. TEM images of PS (a), HSNPs (c), and PSPMA-g-HSNPs (d); SEM image of PS (b); EDXS spectra of HSNPs (e) and PSPMA-g-HSNPs (f).

3.6. In Vitro Cytotoxicity. To evaluate in vitro cytotoxicity of PSPMA-g-HSNPs, MTT assay was conducted using HeLa cells. The cells were incubated with different concentrations of PSPMA brushes-grafted HSNPs for 48 h. As shown in Figure 7, the cell viability is over 85% in the range of 50–1000 $\mu\text{g}/\text{mL}$, indicating that the nanoparticles exhibit good biocompatibility to HeLa cells. The results demonstrate that the PSPMA-g-HSNPs are biocompatible, making them suitable for biomedical applications.

3.7. Rheological Characterization. To evaluate the as-prepared particles as synthetic aqueous lubricants, the rheological properties were first studied (Figure 8). Figure 8a shows the rheological curves of the PSPMA-g-HSNPs aqueous suspensions (0.3 wt %). The viscosity increases gradually with increasing shear rate, indicating that the nanoparticle suspensions can be classified as the shear thickening type of the non-Newtonian fluid. Without shear stress, the particle system was close to the most compact arrangement. When the shear stress acted on the particle system, the relative motion

between the two layers results in the deviation from the most close-packed position and the volume of the dispersion system was increased. If the particles were used as the additive in aqueous lubrication, the decrease of the systemic viscosity under the high-speed friction can be avoided.

Figure 8b shows the plots of storage moduli G' and loss moduli G'' as a function of shear stress at a frequency of 1 Hz. It is clear that G' and G'' both have the plateau regions of the dynamic moduli, and G'' is larger than G' over the entire shear process. The result demonstrated that the particle dispersion system can be assigned to the viscous fluid and had a characteristic viscous deformation under the shear stress, which is the same as the lubricating oil. In spite of their rigid silica layer, PSPMA-g-HSNPs still can maintain the performance of the viscous fluid after the grafting of the PSPMA brushes. Rheological analysis demonstrated that the PSPMA brushes-grafted HSNP dispersions have a great potential for aqueous lubrication.

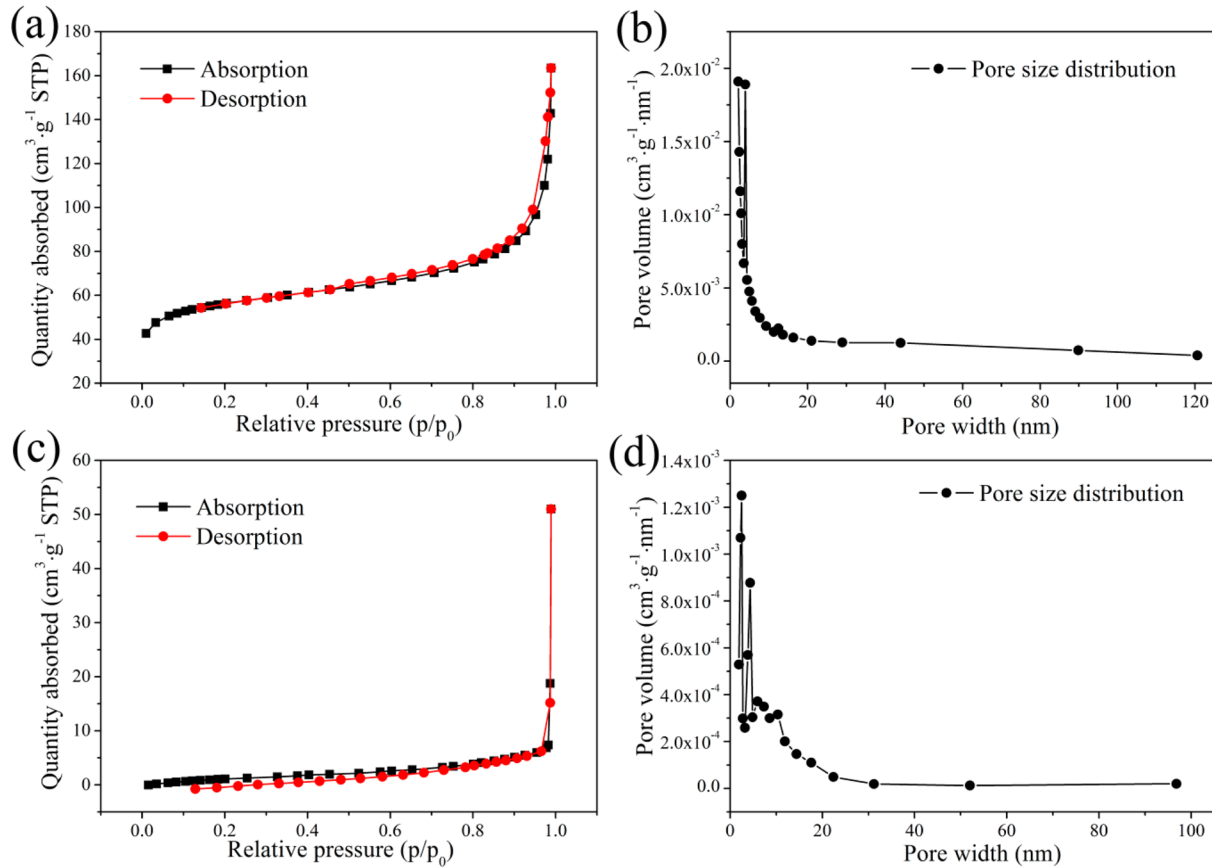


Figure 5. N₂ adsorption–desorption isotherm and pore size distribution curves of HSNPs (a, b) and PSPMA-g-HSNPs (c, d).

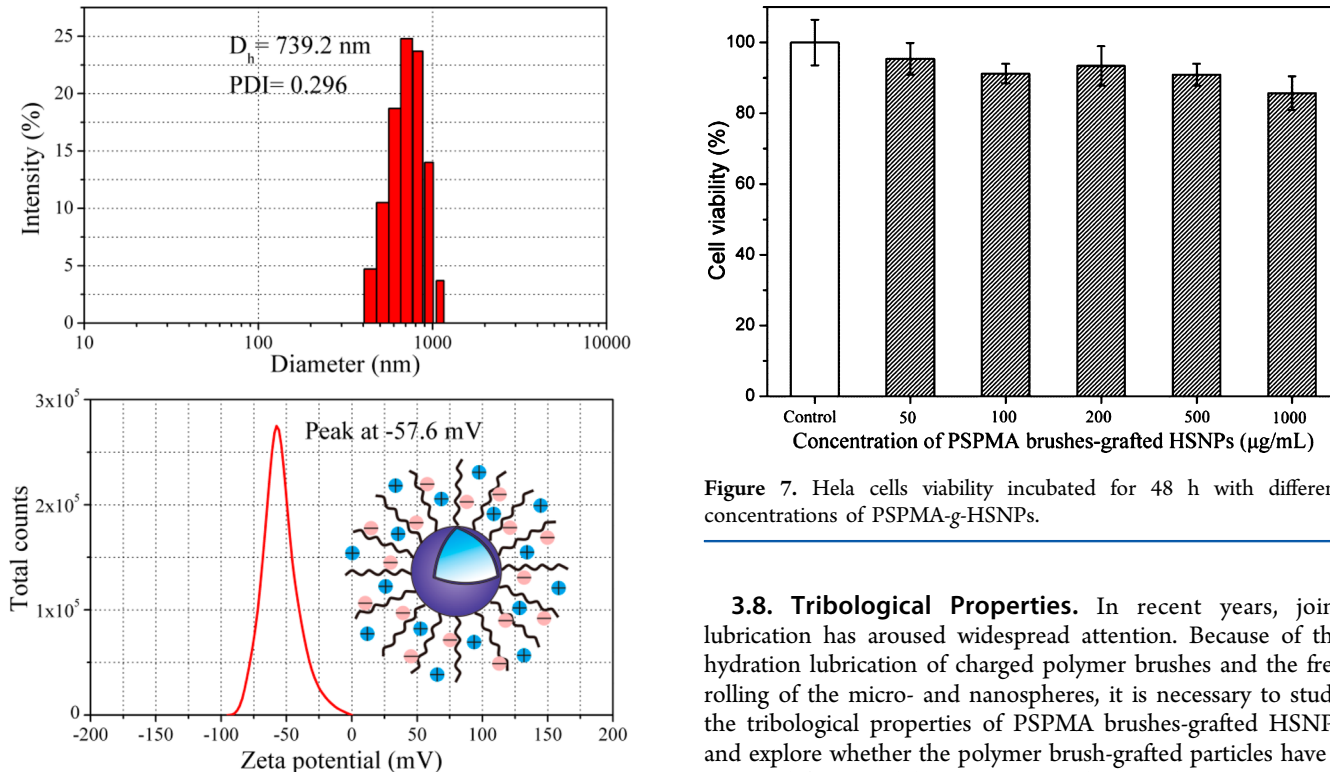


Figure 6. Hydrodynamic diameter distribution (a) and ζ -potential distribution (b) of PSPMA-g-HSNPs in aqueous media at 25 °C.

Figure 7. Hela cells viability incubated for 48 h with different concentrations of PSPMA-g-HSNPs.

3.8. Tribological Properties. In recent years, joint lubrication has aroused widespread attention. Because of the hydration lubrication of charged polymer brushes and the free rolling of the micro- and nanospheres, it is necessary to study the tribological properties of PSPMA brushes-grafted HSNPs and explore whether the polymer brush-grafted particles have a potential for joint-lubricating materials. In order to investigate the tribological properties of PSPMA-g-HSNP aqueous suspensions, the friction and wear tests were carried out on an Optimol SRV-IV oscillating reciprocating friction and wear tester (Figure 9).

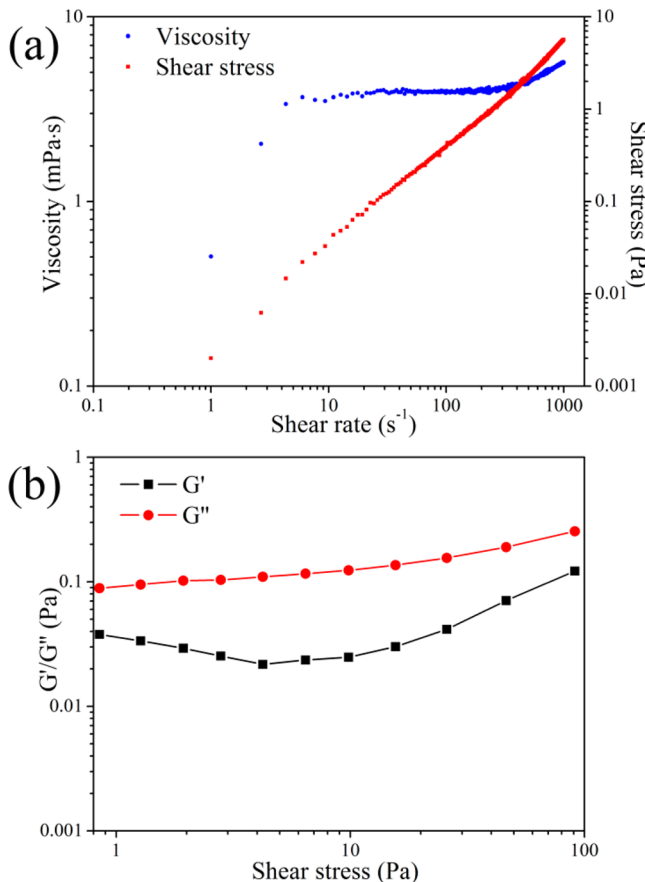


Figure 8. (a) Rheological curves of the PSPMA-g-HSNP aqueous suspensions (0.3 wt %). (b) Plots of storage moduli G' and loss moduli G'' as a function of shear stress at a frequency of 1 Hz.

Figure 9a,b shows the friction curves and wear volumes for steel–steel contacts lubricated by pure water and PSPMA-g-HSNP suspension with different solid contents (0.1, 0.3, and 0.5 wt %) under a normal load of 50 N. It is clear that the addition of PSPMA-g-HSNPs can greatly reduce the friction coefficient and wear volume between steel–steel contacts in comparison with those of the pure water. Meanwhile, the good lubrication effect is improved gradually with the concentration of PSPMA-g-HSNPs. Figure S1a,b of Supporting Information exhibit three-dimensional topography images of pure water and PSPMA-g-HSNP suspension (0.3 wt %) under a normal load of 50 N, intuitively indicating the decrease of wear volume after the addition of PSPMA-g-HSNPs. The friction coefficients were calculated to be 0.345 (pure water), 0.198 (0.1 wt %), 0.187 (0.3 wt %), and 0.173 (0.5 wt %), and correspondingly the wear volumes were 16.96×10^{-4} , 10.92×10^{-4} , 8.98×10^{-4} , and $8.02 \times 10^{-4} \text{ mm}^3$.

After the addition of PSPMA-g-HSNPs, the charged polymer brushes, PSPMA brushes, can form hydrated layers in water and achieve hydration lubrication. Hydration layers formed by polar groups and water molecules can support a large pressure and relax very rapidly and thus cannot be extruded; at the same time, they give a fluid response to shear.^{49,50} In order to weaken the self-energy of enclosed charges, the water molecules surrounding the ion are very tenaciously attached. Thus, the hydration layer is difficult to squeeze out of friction surfaces. At the same time, because of the fast relaxation of water in the hydration layer, the captured counterions can serve as

remarkable lubricants. Because the charge density of charged polymer brushes is larger than that of random charged polymers, the charged polymer brushes have a hydration capability stronger than that of random charged polymers. In addition, PSPMA-g-HSNPs increased the viscosity of pure water, and importantly the viscosity had a gradual increase with the shear rate. It can be conjectured that the free rolling of PSPMA-g-HSNP spheres may employ a “rolling” mechanism to reduce friction between sliding surfaces. The low friction coefficient was achieved by the combination of hydration lubrication and rolling lubrication.

As shown in Figure 9c,d, the friction coefficient and wear volume both increased gradually with the normal load from 50 to 200 N. Under the normal load of 50 to 100 N, the curves of friction coefficient have no apparent fluctuation and the value of friction coefficient is small, suggesting a stable and efficient lubrication. When the normal load reached 150 and 200 N, significant fluctuation appeared in the curves of the friction coefficient and the value of friction coefficient became large, indicating that the as-prepared particles cannot maintain good lubrication above the normal load of 150 N. The friction coefficients were calculated to be 0.187 (50 N), 0.201 (100 N), 0.223 (150 N), and 0.254 (200 N), and correspondingly the wear volumes were 8.98×10^{-4} , 11.92×10^{-4} , 14.97×10^{-4} , and $17.02 \times 10^{-4} \text{ mm}^3$. This result suggests that PSPMA-g-HSNPs can be used as an additive of aqueous lubrication below a certain normal load. The tribological property of PSPMA-g-HSNPs as a function of frequency was also investigated and shown in Figure 9e. As the frequency increases from 5 to 45 Hz, the friction coefficient and wear volume both decreased gradually. In brief, with increasing sliding speed or viscosity, the friction coefficient decreased. In contrast, with increasing normal load, the friction coefficient increased. Considering the typical Stribeck curve shown in Figure 9f, the lubrication system using PSPMA-g-HSNP aqueous suspension can be assigned to the boundary lubrication.

3.9. Absorption Study by Fluorescence Microscopy. In tribology, it is important to study the absorption of lubricants on the surface of friction pairs. It is well-known that Rhodamine B can be chosen as a fluorescent dye for labeling and detecting a substance of interest. In our work, PSPMA-g-HSNPs were dyed by RHB through electrostatic interaction. The absorption of PSPMA-g-HSNPs on the steel–steel contacts was studied by fluorescence microscopy using a previously described method.⁵² The fluorescence imaging of the surface of steel blocks incubated with RHB-labeled PSPMA-g-HSNPs is displayed in Figure 10. It is clear that there are obvious fluorescence spots appearing on the surface of steel blocks, indicating that the steel block has a strong absorption for PSPMA-g-HSNPs. In addition, with increasing concentration of PSPMA-g-HSNPs, the absorption phenomenon was enhanced gradually. Because of the relatively high surface energy of iron atoms, PSPMA-g-HSNPs can be chemically absorbed on the surface of fresh steel block easily to form a thin absorption film, which was employed as a protective boundary film to achieve boundary lubrication. The results demonstrated that the tribological system lubricated by PSPMA-g-HSNP aqueous suspension was composed of hydration lubrication in aqueous media and boundary lubrication formed by the absorption film.

3.10. In Vitro Drug Loading and Release Behavior. Because the medium of the biological systems is water, hydration lubrication plays an important role in the biological lubrication. Because of good hydration effect in aqueous

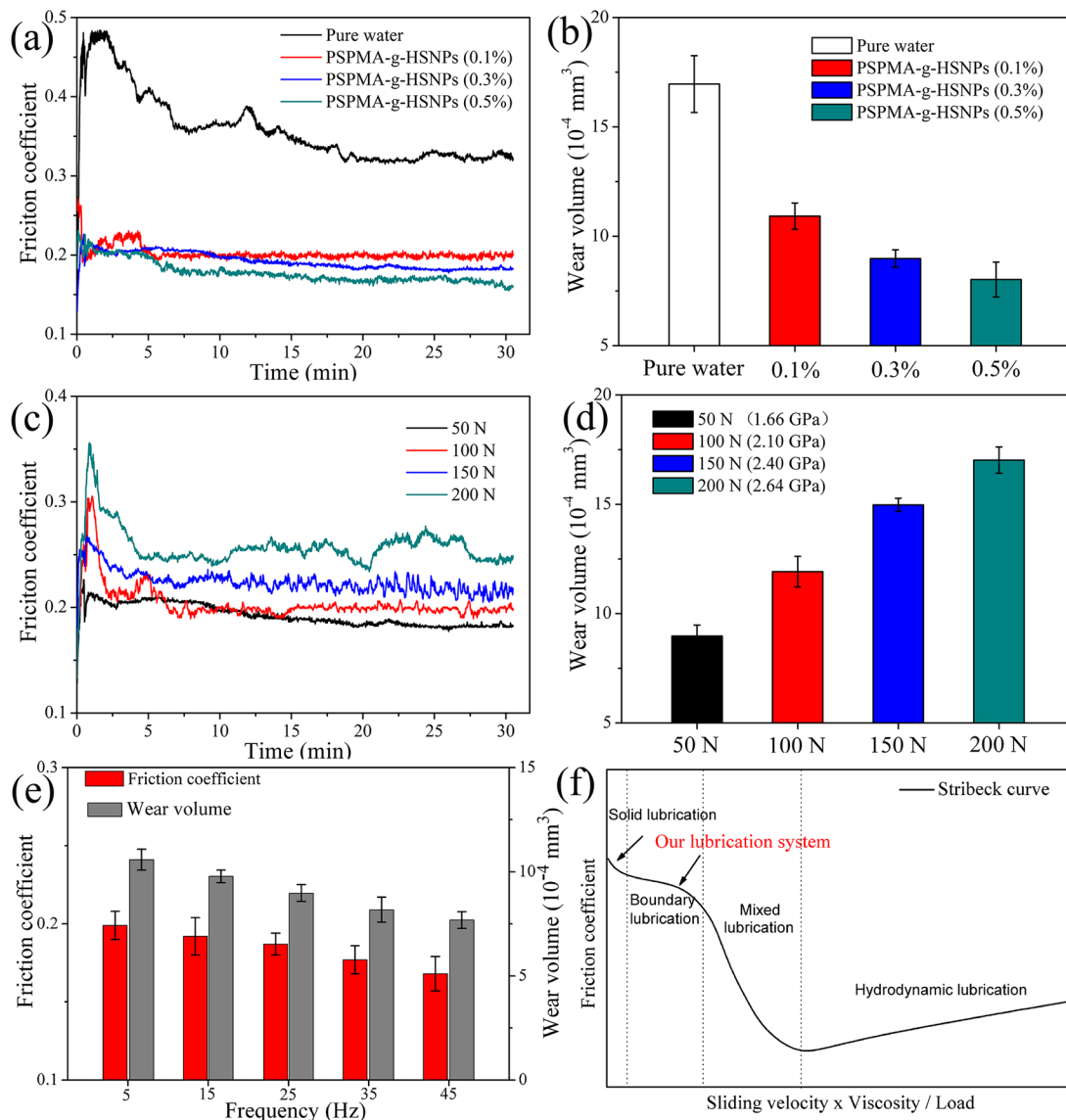


Figure 9. Friction curves (a) and wear volumes (b) for steel–steel contacts lubricated by pure water and PSPMA-g-HSNP suspension with different solid contents (0.1, 0.3, and 0.5 wt %). Friction curves (c) and wear volumes (d) for steel–steel contacts lubricated by PSPMA-g-HSNP dispersion (0.3 wt %) as a function of normal load. (e) Friction coefficient and wear volume for steel–steel contacts lubricated by PSPMA-g-HSNP dispersion (0.3 wt %) as a function of frequency. (f) Typical stribeck curve⁵¹ used for defining our lubrication system.

solution, charged polymer brushes may be a promising candidate for biological friction. In this case, the good biocompatibility of the as-prepared PSPMA-g-HSNPs may provide a potential application for artificial joint lubrication. In addition, because of the interior cavity and superficial pores of HSNPs, PSPMA-g-HSNPs can be employed as a drug carrier for joint treatment.

Aspirin has anti-inflammatory, analgesic, and antipyretic effects and is a specific drug for arthritis and rheumatism. Herein, we used PSPMA-g-HSNPs to load aspirin, and PSPMA-g-HSNPs/aspirin composites may achieve the double effect of joint lubrication and disease treatment. The aspirin-loaded PSPMA-g-HSNPs were obtained after stirring for 48 h and centrifugation at the speed of 8000 rpm for 5 min. The calculated drug loading capacity and encapsulation efficiency were 35.4% and 54.7%, respectively, which demonstrates that the PSPMA-g-HSNPs have a good drug loading capacity.

The calibration curve of aspirin was used to calculate the amount of aspirin release (Figure S2 of Supporting Information). Figure 11 shows the release profiles of free aspirin, aspirin-loaded HSNPs, and aspirin-loaded PSPMA brushes-grafted HSNPs. It is found that the accumulated amount of aspirin without a carrier rapidly reached 100% within 5 h. When the HSNPs were used as the nanocarrier, 83.2 % and 87.4 % of aspirin were released within 24 and 72 h, respectively. However, when the PSPMA brushes-grafted HSNPs were employed as the nanocarrier, 67.0 % and 74.5 % of aspirin were released within 24 and 72 h, respectively. When the two release curves of aspirin-loaded HSNPs and aspirin-loaded PSPMA brushes-grafted HSNPs are compared, the amount of IBU released from PSPMA brushes-grafted HSNPs is always smaller than that from HSNPs at all intervals.

In comparison with the release profile of free aspirin, aspirin-loaded HSNPs and aspirin-loaded PSPMA-g-HSNPs both exhibited significant sustained-release behavior. However,

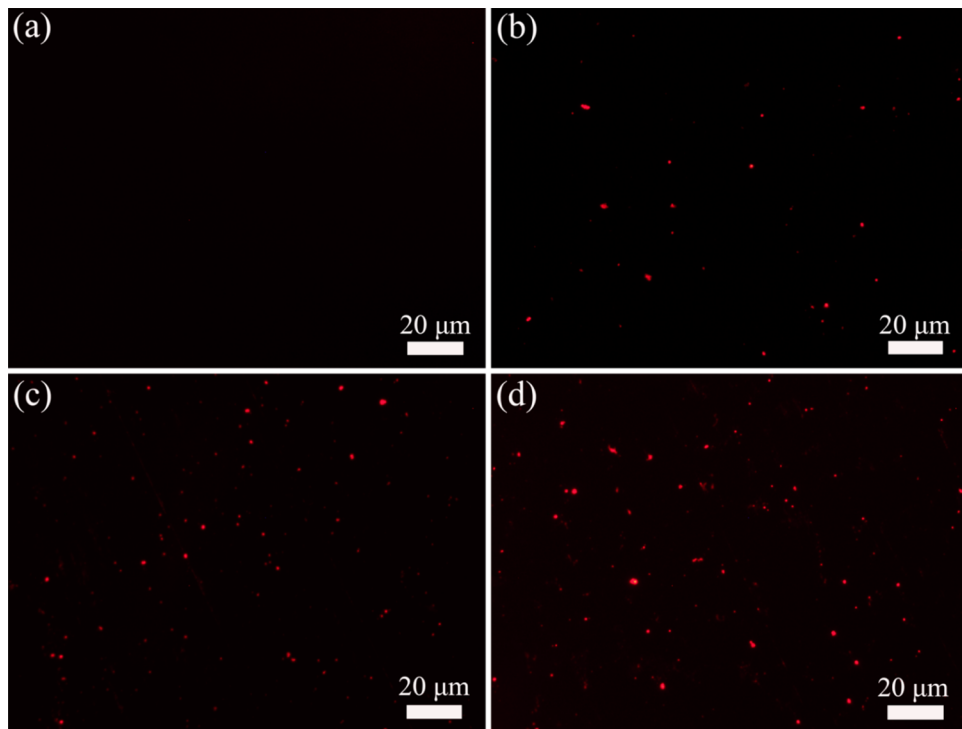


Figure 10. Fluorescent images of the surfaces of steel blocks incubated for 1.0 h by RHB-labeled PSPMA-g-HSNP suspension with different concentrations: (a) blank control, (b) 0.1 wt %, (c) 0.3 wt %, and (d) 0.5 wt %.

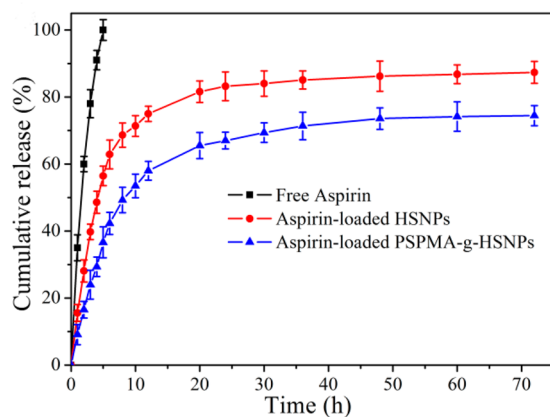


Figure 11. Release profiles of free aspirin, aspirin-loaded HSNPs, and aspirin-loaded PSPMA-g-HSNPs in PBS buffer solutions (pH 7.4) at the human physiological temperature (37 °C).

because of the coverage of PSPMA polymer brushes, PSPMA-g-HSNPs have a better sustained-release performance for aspirin. In dry conditions, the drug can be completely encapsulated in the interior cavity of PSPMA brushes-grafted HSNPs because of the collapse of polymer brushes. In aqueous conditions, the loaded drug can be released to the outside through the pores of HSNPs because of the swelling of the superhydrophilic charged polymer brushes. Herein, PSPMA brushes act as the “switch” for aspirin in and out, responding to an aqueous media. The in vitro drug loading and release study demonstrates that PSPMA brushes-grafted HSNPs can be used as a nanocarrier to achieve sustained-release for aspirin in the human physiological environment.

In general, artificial drug nanocarriers contain soft polymer nanoparticles (including microgels, colloids, and self-assembled

micelles) and rigid inorganic nanoparticles (including silica spheres, Au nanoparticles, and graphenes). The former will undergo a severe deformation in aqueous lubrication because of the large normal load, resulting in a fast release of drugs. Fortunately, the latter can sustain a larger normal load, avoiding the undesirable deformation and maintaining the sustained-release for the drug in the friction process. For PSPMA-g-HSNPs, the rigid silica cores can prevent aspirin from being squeezed out quickly. In vitro drug loading and release were conducted using aspirin as a model drug in the human physiological environment, indicating the suitability of PSPMA-g-HSNPs as a drug loading and sustained-release carrier.

These results show that the obtained composite nanoparticles, PSPMA brushes-grafted HSNPs, have a great potential as an injectable joint lubricant fluid in therapy treatment.

4. CONCLUSION

We have introduced a novel type of multifunctional nanoparticles for both hydration lubrication and drug delivery system. The core/shell charged polymer brushes-grafted hollow silica particles, PSPMA-g-HSNPs, were successfully fabricated by surface-initiated ATRP. HSNPs with a silica shell of ca. 28 nm were coated by a polymer brush layer of ca. 40 nm. PSPMA brushes have a strong hydration capability, and PSPMA brushes-grafted HSNPs exhibit a good swelling behavior in aqueous media. Rheological characterization, tribological tests, and absorption analysis suggest a good hydration lubricating effect of the composite nanoparticles. When a drug (aspirin was used as a model drug) was encapsulated inside the hollow nanoparticles, a significant sustained release for aspirin was achieved. The combination of hydration lubrication and drug loading capability renders the core/shell charged polymer

brushes-grafted hollow silica particles a promising material for joint lubrication and arthritis treatment.

■ ASSOCIATED CONTENT

Supporting Information

Three-dimensional topography images of pure water and PSPMA brushes-grafted HSNNPs suspension (0.3 wt %) under a normal load of 50 N and the calibration curve of aspirin based on the UV absorption. This material is available free of charge via the Internet at <http://pubs.acs.org>.

■ AUTHOR INFORMATION

Corresponding Authors

*E-mail: cmr2611529@gmail.com. Phone: +86 0931 4968045.

*E-mail: zhouf@licp.cas.cn. Phone: +86 0931 4968466.

Notes

The authors declare no competing financial interest.

■ ACKNOWLEDGMENTS

The authors are grateful for the financial support from NSFC (21125316, 21204095, 51335010), 973 projects (2013CB632300), and Key Research Program of CAS (KJZD-EW-M01).

■ REFERENCES

- (1) Neu, C. P.; Komvopoulos, K.; Reddi, A. H. The Interface of Functional Biotribology and Regenerative Medicine in Synovial Joints. *Tissue Eng., Part B* **2008**, *14*, 235–247.
- (2) Waller, K. A.; Zhang, L. X.; Elsaied, K. A.; Fleming, B. C.; Warman, M. L.; Jay, G. D. Role of Lubricin and Boundary Lubrication in the Prevention of Chondrocyte Apoptosis. *Proc. Natl. Acad. Sci. U.S.A.* **2013**, *110*, 5852–5857.
- (3) Klein, J. Repair or Replacement—A Joint Perspective. *Science* **2009**, *323*, 47–48.
- (4) Sivan, S.; Schroeder, A.; Verberne, G.; Merkher, Y.; Diminsky, D.; Priev, A.; Maroudas, A.; Halperin, G.; Nitzan, D.; Etsion, I.; et al. Liposomes Act as Effective Biolubricants for Friction Reduction in Human Synovial Joints. *Langmuir* **2010**, *26*, 1107–1116.
- (5) Wathier, M.; Lakin, B. A.; Bansal, P. N.; Stoddart, S. S.; Snyder, B. D.; Grinstaff, M. W. A Large-Molecular-Weight Polyanion, Synthesized via Ring-Opening Metathesis Polymerization, as a Lubricant for Human Articular Cartilage. *J. Am. Chem. Soc.* **2013**, *135*, 4930–4933.
- (6) Ghosh Chaudhuri, R.; Paria, S. Core/Shell Nanoparticles: Classes, Properties, Synthesis Mechanisms, Characterization, and Applications. *Chem. Rev. (Washington, DC, U.S.)* **2012**, *112*, 2373–2433.
- (7) Zhu, H.; Tao, J.; Wang, W.; Zhou, Y.; Li, P.; Li, Z.; Yan, K.; Wu, S.; Yeung, K. W.; Xu, Z.; et al. Magnetic, Fluorescent, and Thermo-Responsive Fe_3O_4 /Rare Earth Incorporated Poly(St-NIPAM) Core-Shell Colloidal Nanoparticles in Multimodal Optical/Magnetic Resonance Imaging Probes. *Biomaterials* **2013**, *34*, 2296–2306.
- (8) Chen, Y.; Li, X. Near-Infrared Fluorescent Nanocapsules with Reversible Response to Thermal/pH Modulation for Optical Imaging. *Biomacromolecules* **2011**, *12*, 4367–4372.
- (9) Kabachii, Y. A.; Golub, A. S.; Kochev, S. Y.; Lenenko, N. D.; Abramchuk, S. S.; Antipin, M. Y.; Valetsky, P. M.; Stein, B. D.; Mahmoud, W. E.; Al-Ghamdi, A. A.; et al. Multifunctional Nano-hybrids by Self-Assembly of Monodisperse Iron Oxide Nanoparticles and Nanolamellar MoS_2 Plates. *Chem. Mater.* **2013**, *25*, 2434–2440.
- (10) Zhang, F.; Braun, G. B.; Shi, Y.; Zhang, Y.; Sun, X.; Reich, N. O.; Zhao, D.; Stucky, G. Fabrication of $\text{Ag}@\text{SiO}_2@Y_2\text{O}_3:\text{Er}$ Nanostructures for Bioimaging: Tuning of the Upconversion Fluorescence with Silver Nanoparticles. *J. Am. Chem. Soc.* **2010**, *132*, 2850–2851.
- (11) Zou, H.; Wu, S.; Shen, J. Polymer/Silica Nanocomposites: Preparation, Characterization, Properties, and Applications. *Chem. Rev. (Washington, DC, U.S.)* **2008**, *108*, 3893–3957.
- (12) Kyomoto, M.; Moro, T.; Saiga, K.; Hashimoto, M.; Ito, H.; Kawaguchi, H.; Takatori, Y.; Ishihara, K. Biomimetic Hydration Lubrication with Various Polyelectrolyte Layers on Cross-Linked Polyethylene Orthopedic Bearing Materials. *Biomaterials* **2012**, *33*, 4451–4459.
- (13) Yasuda, K.; Ping Gong, J.; Katsuyama, Y.; Nakayama, A.; Tanabe, Y.; Kondo, E.; Ueno, M.; Osada, Y. Biomechanical Properties of High-Toughness Double Network Hydrogels. *Biomaterials* **2005**, *26*, 4468–4475.
- (14) Dédinaté, A. Biomimetic Lubrication. *Soft Matter* **2012**, *8*, 273–284.
- (15) Jeffrey, D. R. Imaging Hyaline Cartilage. *Br. J. Radiol.* **2003**, *76*, 777–787.
- (16) Klein, J. Hydration Lubrication. *Friction* **2013**, *1*, 1–23.
- (17) Briscoe, W. H.; Titmuss, S.; Tiberg, F.; Thomas, R. K.; McGillivray, D. J.; Klein, J. Boundary Lubrication under Water. *Nature (London, U.K.)* **2006**, *444*, 191–194.
- (18) Gaisinskaya, A.; Ma, L.; Silbert, G.; Sorkin, R.; Tairy, O.; Goldberg, R.; Kampf, N.; Klein, J. Hydration Lubrication: Exploring a New Paradigm. *Faraday Discuss.* **2012**, *156*, 217–233.
- (19) Jin, Z.; Dowson, D. Bio-Friction. *Friction* **2013**, *1*, 100–113.
- (20) Sorkin, R.; Kampf, N.; Dror, Y.; Shimoni, E.; Klein, J. Origins of Extreme Boundary Lubrication by Phosphatidylcholine Liposomes. *Biomaterials* **2013**, *34*, 5465–5475.
- (21) Chen, M.; Briscoe, W. H.; Armes, S. P.; Klein, J. Lubrication at Physiological Pressures by Polyzwitterionic Brushes. *Science* **2009**, *323*, 1698–1701.
- (22) Raviv, U.; Giasson, S.; Kampf, N.; Gohy, J.-F. o.; Jérôme, R.; Klein, J. Lubrication by Charged Polymers. *Nature (London, U.K.)* **2003**, *425*, 163–165.
- (23) Raviv, U.; Giasson, S.; Kampf, N.; Gohy, J.-F. o.; Jérôme, R.; Klein, J. Normal and Frictional Forces between Surfaces Bearing Polyelectrolyte Brushes. *Langmuir* **2008**, *24*, 8678–8687.
- (24) Landherr, L. J.; Cohen, C.; Agarwal, P.; Archer, L. A. Interfacial Friction and Adhesion of Polymer Brushes. *Langmuir* **2011**, *27*, 9387–9395.
- (25) Kobayashi, M.; Terada, M.; Takahara, A. Polyelectrolyte Brushes: A Novel Stable Lubrication System in Aqueous Conditions. *Faraday Discuss.* **2012**, *156*, 403–412.
- (26) Nomura, A.; Goto, A.; Ohno, K.; Kayahara, E.; Yamago, S.; Tsujii, Y. Controlled Synthesis of Hydrophilic Concentrated Polymer Brushes and Their Friction/Lubrication Properties in Aqueous Solutions. *J. Polym. Sci., Part A: Polym. Chem.* **2011**, *49*, 5284–5292.
- (27) Spirin, L.; Galuschnko, A.; Kreer, T.; Binder, K.; Baschnagel, J. Polymer-Brush Lubricated Surfaces with Colloidal Inclusions under Shear Inversion. *Phys. Rev. Lett.* **2011**, *106*, 168301–168304.
- (28) Peng, D. X.; Kang, Y.; Hwang, R. M.; Shyr, S. S.; Chang, Y. P. Tribological Properties of Diamond and SiO_2 Nanoparticles Added in Paraffin. *Tribol. Int.* **2009**, *42*, 911–917.
- (29) Frishberg, I. V.; Kishkoparov, N. V.; Zolotukhina, L. V.; Kharlamov, V. V.; Baturina, O. K.; Zhidovinova, S. V. Effect of Ultrafine Powders in Lubricants on Performance of Friction Pairs. *Wear* **2003**, *254*, 645–651.
- (30) Kim, D.; Archer, L. A. Nanoscale Organic–Inorganic Hybrid Lubricants. *Langmuir* **2011**, *27*, 3083–3094.
- (31) Zhang, Q.; Archer, L. A. Interfacial Friction of Surfaces Grafted with One- and Two-Component Self-Assembled Monolayers. *Langmuir* **2005**, *21*, 5405–5413.
- (32) Gao, T.; Jelle, B. P.; Sandberg, L. I.; Gustavsen, A. Monodisperse Hollow Silica Nanospheres for Nano Insulation Materials: Synthesis, Characterization, and Life Cycle Assessment. *ACS Appl. Mater. Interfaces* **2013**, *5*, 761–767.
- (33) Nagase, K.; Kobayashi, J.; Kikuchi, A.; Akiyama, Y.; Kanazawa, H.; Okano, T. High Stability of Thermoresponsive Polymer-Brush-Grafted Silica Beads as Chromatography Matrices. *ACS Appl. Mater. Interfaces* **2012**, *4*, 1998–2008.
- (34) Zhao, L.; Qin, H.; Hu, Z.; Zhang, Y.; Wu, R. a.; Zou, H. A Poly(Ethylene Glycol)-Brush Decorated Magnetic Polymer for Highly

Specific Enrichment of Phosphopeptides. *Chem. Sci.* **2012**, *3*, 2828–2838.

(35) Zhuang, Y.; Zhu, Q.; Tu, C.; Wang, D.; Wu, J.; Xia, Y.; Tong, G.; He, L.; Zhu, B.; Yan, D.; et al. Protein Resistant Properties of Polymers with Different Branched Architecture on a Gold Surface. *J. Mater. Chem.* **2012**, *22*, 23852–23860.

(36) Li, G. L.; Zheng, Z.; hwald, H. M.; Shchukin, D. G. Silica/Polymer Double-Walled Hybrid Nanotubes: Synthesis and Application as Stimuli-Responsive Nanocontainers in Self-Healing Coatings. *ACS Nano* **2013**, *7*, 2470–2478.

(37) Farrukh, A.; Akram, A.; Ghaffar, A.; Hanif, S.; Hamid, A.; Duran, H.; Yameen, B. Design of Polymer-Brush-Grafted Magnetic Nanoparticles for Highly Efficient Water Remediation. *ACS Appl. Mater. Interfaces* **2013**, *5*, 3784–3793.

(38) Yan, J.; Li, B.; Yu, B.; Huck, W. T.; Liu, W.; Zhou, F. Controlled Polymer-Brush Growth from Microliter Volumes Using Sacrificial-Anode Atom-Transfer Radical Polymerization. *Angew. Chem., Int. Ed.* **2013**, *52*, 9125–9129.

(39) Li, B.; Yu, B.; Huck, W. T.; Zhou, F.; Liu, W. Electrochemically Induced Surface-Initiated Atom-Transfer Radical Polymerization. *Angew. Chem., Int. Ed.* **2012**, *51*, 5092–5095.

(40) Cao, S.; Fang, L.; Zhao, Z.; Ge, Y.; Piletsky, S.; Turner, A. P. F. Hierarchically Structured Hollow Silica Spheres for High Efficiency Immobilization of Enzymes. *Adv. Funct. Mater.* **2013**, *23*, 2162–2167.

(41) Deng, Z.; Zhen, Z.; Hu, X.; Wu, S.; Xu, Z.; Chu, P. K. Hollow Chitosan-Silica Nanospheres as pH-Sensitive Targeted Delivery Carriers in Breast Cancer Therapy. *Biomaterials* **2011**, *32*, 4976–4986.

(42) Li, Z.; Barnes, J. C.; Bosoy, A.; Stoddart, J. F.; Zink, J. I. Mesoporous Silica Nanoparticles in Biomedical Applications. *Chem. Soc. Rev.* **2012**, *41*, 2590–2605.

(43) Liberman, A.; Martinez, H. P.; Ta, C. N.; Barback, C. V.; Mattrey, R. F.; Kono, Y.; Blair, S. L.; Troglar, W. C.; Kummel, A. C.; Wu, Z. Hollow Silica and Silica-Boron Nano/Microparticles for Contrast-Enhanced Ultrasound to Detect Small Tumors. *Biomaterials* **2012**, *33*, 5124–5129.

(44) Tang, F.; Li, L.; Chen, D. Mesoporous Silica Nanoparticles: Synthesis, Biocompatibility and Drug Delivery. *Adv. Mater.* **2012**, *24*, 1504–1534.

(45) Chen, M.; Wu, L.; Zhou, S.; You, B. A Method for the Fabrication of Monodisperse Hollow Silica Spheres. *Adv. Mater.* **2006**, *18*, 801–806.

(46) Deng, Z.; Chen, M.; Zhou, S.; You, B.; Wu, L. A Novel Method for the Fabrication of Monodisperse Hollow Silica Spheres. *Langmuir* **2006**, *22*, 6403–6407.

(47) Gong, X. Q.; Peng, S. L.; Wen, W. J.; Sheng, P.; Li, W. H. Design and Fabrication of Magnetically Functionalized Core/Shell Microspheres for Smart Drug Delivery. *Adv. Funct. Mater.* **2009**, *19*, 292–297.

(48) Wu, J.; Zhu, Y. J.; Cao, S. W.; Chen, F. Hierachically Nanostructured Mesoporous Spheres of Calcium Silicate Hydrate: Surfactant-Free Sonochemical Synthesis and Drug-Delivery System with Ultrahigh Drug-Loading Capacity. *Adv. Mater.* **2010**, *22*, 749–753.

(49) Raviv, U.; Laurat, P.; Klein, J. Fluidity of Water Confined to Subnanometre Films. *Nature (London, U.K.)* **2001**, *413*, 51–54.

(50) Raviv, U.; Perkin, S.; Laurat, P.; Klein, J. Fluidity of Water Confined Down to Subnanometer Films. *Langmuir* **2004**, *20*, 5322–5332.

(51) Kondo, Y.; Koyama, T.; Sasaki, S. Tribological Properties of Ionic Liquids. In *Ionic Liquids – New Aspects for the Future*; Kadokawa, J.-i., Ed.; InTech: Japan, 2013.

(52) Roba, M.; Naka, M.; Gautier, E.; Spencer, N. D.; Crockett, R. The Adsorption and Lubrication Behavior of Synovial Fluid Proteins and Glycoproteins on the Bearing-Surface Materials of Hip Replacements. *Biomaterials* **2009**, *30*, 2072–2078.